Thermal and Mechanical Test Methods and Behavior of CONTINUOUS-FIBER CERAMIC COMPOSITES

Michael G. Jenkins
Stephen T. Gonczy
Edgar Lara-Curzio
Noel E. Ashbaugh
Larry P. Zawada
Editors

ASTM STP 1309

STP 1309

Thermal and Mechanical Test Methods and Behavior of Continuous-Fiber Ceramic Composites

Michael G. Jenkins, Edgar Lara-Curzio, Stephen T. Gonczy, Noel E. Ashbaugh, and Larry P. Zawada, Editors

ASTM Publication Code Number (PCN):
04-013090-30

ASTM
100 Barr Harbor Drive
West Conshohocken, PA 19428-2959

Printed in the U.S.A.

ISBN: 0-8031-2033-8
PCN: 04-013090-30

Photocopy Rights

Peer Review Policy

Each paper published in this volume was evaluated by two peer reviewers and at least one of the Editors. The authors addressed all of the reviewers' comments to the satisfaction of both the technical editor(s) and the ASTM Committee on Publications.

To make technical information available as quickly as possible, the peer-reviewed papers in this publication were prepared "camera-ready" as submitted by the authors.

The quality of the papers in this publication reflects not only the obvious efforts of the authors and the technical editor(s), but also the work of these peer reviewers. The ASTM Committee on Publications acknowledges with appreciation their dedication and contribution of time and effort on behalf of ASTM.

Printed in Philadelphia, PA
March 1997

Foreword

This publication, *Thermal and Mechanical Test Methods and Behavior of Continuous-Fiber Ceramic Composites,* contains papers presented at the symposium of the same name held in Cocoa Beach, Florida on 8-9 Jan. 1996. The symposium was sponsored by ASTM Committee C28 on Advanced Ceramics, ASTM Committee E08 on Fatigue and Fracture, and the American Ceramic Society, Engineering Ceramics Division. Michael G. Jenkins, University of Washington, Edgar Lara-Curzio, Oak Ridge National Laboratory, Stephen T. Gonczy, Gateway Materials Technology, Noel E. Ashbaugh, University of Dayton Research Institute, and Larry P. Zawada, Wright Laboratory, presided as symposium cochairmen and are also the editors of the resulting publication.

Contents

Nondestructive Characterization

Modeling and Processing

Testing of Tubes

Room-Temperature Test Results/Methods

John P. Piccola, Jr.,[1] Michael G. Jenkins,[2] and Edgar Lara-Curzio[3]

INFLUENCE OF TEST MODE, TEST RATE, SPECIMEN GEOMETRY, AND BENDING ON TENSILE MECHANICAL BEHAVIOR OF A CONTINUOUS FIBER CERAMIC COMPOSITE

REFERENCE: Piccola, J. P., Jr., Jenkins, M. G., and Lara-Curzio, E., **"Influence of Test Mode, Test Rate, Specimen Geometry, and Bending on Tensile Mechanical Behavior of a Continuous Fiber Ceramic Composite,"** Thermal and Mechanical Test Methods and Behavior of Continuous-Fiber Ceramic Composites, ASTM STP 1309, Michael G. Jenkins, Stephen T. Gonczy, Edgar Lara-Curzio, Noel E. Ashbaugh, and Larry P. Zawada, Eds., American Society for Testing and Materials, 1997.

ABSTRACT: ASTM Test Method for Monotonic Tensile Strength Testing of Continuous Fiber-Reinforced Advanced Ceramics with Solid Rectangular Cross-Section Specimens at Ambient Temperatures (C 1275) was used to investigate the effects of test mode (load versus displacement), test rate (fast versus slow), specimen geometry (straight-sided versus reduced-gage section), specimen volume (long/thin versus short/fat), and bending in tension for a twelve-ply, two-dimensional, plain weave SiC fiber reinforced / SiC matrix continuous fibre ceramic composite. Although it appeared that "graceful failure" is sometimes accentuated by displacement control at slow rates, a two-way analysis of variance (ANOVA) with replication at the 95% significance level of all the test results showed that there was no significance of test rate, test mode or specimen geometry for proportional limit stress. Similarly, for ultimate tensile strength there was no significance of test rate or test mode although there was a significance of specimen geometry. Finally, for this two dimensional, plain weave fiber architecture there was no significance of test rate, test mode, or specimen geometry (including straight-sided specimens) on fracture location. Proportional limit stress decreased with increasing bending while ultimate tensile strength appeared independent of bending.

KEYWORDS: continuous fiber ceramic composite, tension test, bending, test rate, test mode, specimen volume, proportional limit stress, ultimate tensile strength

Continuous fiber ceramic composites (CFCCs) are a relatively new area of composite research. Additional and extensive investigations of

[1]Structural analyst,seats, Boeing Commercial Airplane Group, Seattle, WA 98124-2207.

[2]Assistant professor, Department of Mechanical Engineering, University of Washington, Seattle, WA 98195-2600.

[3]Development staff member, Metals and Ceramics Division, Oak Ridge National Laboratory, Oak Ridge, TN 37831-6064.

various types of CFCCs and other ceramic matrix composites are required before industry adopts CFCCs on a widespread scale [1]. A primary advantage of CFCCs is their inherent damage tolerance (i.e. the increased ability of the material to absorb energy without catastrophic fracture, also known as "toughness"), thereby overcoming the brittleness often associated with ceramics, while maintaining the high-temperature performance of their monolithic counterparts [2,3].

A broad range of industrial sectors have the potential for implementing CFCCs [1] because of the economic and energy considerations. Chemical processing, refining operations, power generation, and heat engines all can benefit from the use of CFCC components such as filters, substrates, piping, tanks, burners, heat pipes, tubes, combustor liners, vanes, and nozzles.

These potential applications have justified the need for additional experimental [4-6] and analytical research [7-9] of CFCCs. However, many of these studies have involved unidirectional composites with glass matrices [4]. Brittle matrix composites reinforced in multiple directions have only recently begun receiving attention [2,5,6]. Experimental work has demonstrated the effect of matrix cracking and the debonding layer between the fibers and the matrix on the strength of the composite [10]. Analytical modeling of these conditions has been performed along with models of the stress-strain behavior [7]. More extensive systematic studies are still lacking to determine the effects on the mechanical properties and performance of such common test parameters as test mode/rate, specimen geometry/volume, and nonuniform stresses (i.e., bending).

A primary motivation for this study was to produce fundamental information the mechanical properties and performance of a two-dimensionally-reinforced CFCC. Additionally, certain recommendations and requirements of the recently introduced test standard ASTM Test Method for Monotonic Tensile Strength Testing of Continuous Fiber-Reinforced Advanced Ceramics with Solid Rectangular Cross-Section Specimens at Ambient Temperatures (C 1275) still require clarification. Thus, a further motivation for this study was to characterize various testing parameters such as test mode, test rate, specimen geometry, etc. and their subsequent effects on the tensile mechanical behavior of a two-dimensional (2D), woven SiC fiber-reinforced / SiC matrix CFCC.

The material is briefly described. An overview of the experimental procedure follows. Test results are presented in terms of stress-strain response, proportional limit stress, ultimate tensile strength and modulus of toughness. The effect of bending on proportional limit stress and ultimate tensile strength is discussed. Fracture location and its relation to specimen geometry is also evaluated. Finally, an analysis of variation (ANOVA) is used to justify pooling of the test results.

TEST MATERIAL

Material Description

A commercial CFCC (SuperTemp from B.F. Goodrich Aerospace, Brecksville, Ohio) was the focus of this study. The 2D-reinforcement was a plain woven cloth of ~1800 denier fiber bundles (~500 fibers/bundle) composed of a ceramic grade (Nicalon™) Si-C-O fiber. The fiber preform was fabricated by layering twelve plies of cloth with the warp of the fibers along the longitudinal direction of the test specimens.

The matrix was processed as follows. In the initial step, chemical vapor infiltration (CVI) was used to deposit a ~0.3 μm interfacial layer of pyrolytic carbon onto the fiber preform. In the final step, methyltrichlorosilane was decomposed, infiltrating the preforms by CVI until all the surface microporosity was filled, thus preventing further CVI of the interior of the material while forming a crystalline β-SiC matrix. The remaining microporosity (~20 to 25 vol%) was primarily located within the internal fiber bundles. The porosity was estimated from bulk density measurements, actual fiber volume fractions, and theoretical density of the CFCC calculated densities of constituent materials. Approximate volume fractions of fibers and matrix were 35% and 40%, respectively.

Tensile Specimens

Simple, straight-sided and reduced gage section (i.e., dog bone) flat specimens were fabricated by an undisclosed process (presumably diamond-grit cutting and grinding) into four different test specimen geometries designated RG1, RG2, RG3, and SS (Fig. 1). The twelve-ply specimens were ~3.7 mm thick.

Tapered (5°) end tabs [6] consisted of an E-glass fiber/epoxy matrix composite were used to protect the specimens from being damaged at the area within the hydraulic grips. Such damage can be in the form of premature splitting due to the contact of the grip surface with the specimen. The ratio of the resin to curing agent was chosen to produce an adhesive with a shear strength greater than ~9.4 MPa, the maximum interfacial shear stress anticipated at the interface of the tab and specimen, so as to prevent delamination at the end tab and subsequent damage to the specimen.

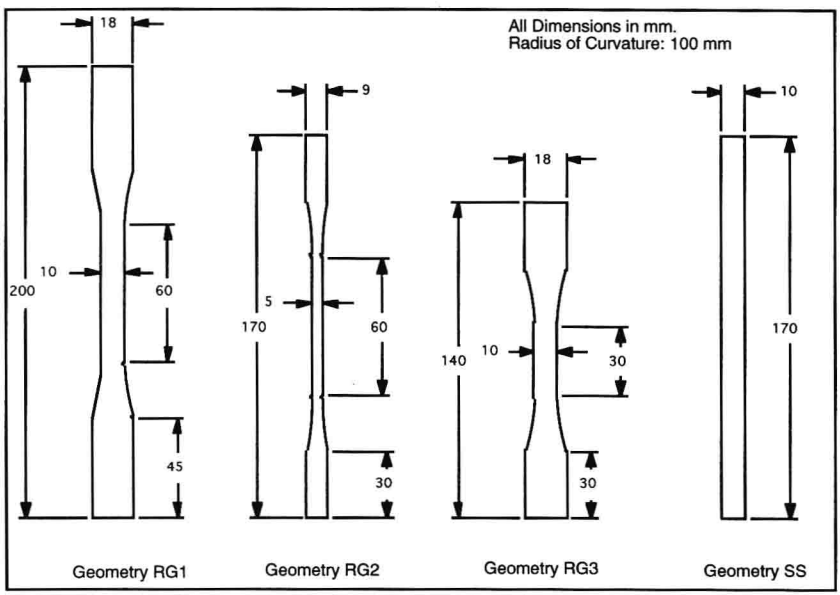

FIG. 1--Specimen geometries for evaluation of geometry effects.

EXPERIMENTAL PROCEDURE

All thirty-two tests were conducted at ambient temperatures (20 to 22°C, 55 to 65 %RH) per ASTM C 1275 on a commercial, single-actuator, electromechanical materials test system (100-kN capacity) having both load and cross-head displacement control capabilities. A digital controller with related software managed all input and output signals.

Commercial, hydraulically-actuated specimen grips were independently activated and could maintain an adjustable grip force on the specimen grip face without backlash. The actual grip faces were coated with a roughened, sputtered WC coating to prevent slippage at the specimen/grip interface. Grips were attached to the load frame via a fixed, but adjustable, commercially available alignment system.

In compliance with ASTM C 1275 verification of load train alignment was performed before and after the series of tests to assure less than 5 percent bending (PB as described in Eq. 1 below) at an average strain of 500 x 10^{-6} m/m in the alignment specimen. A steel alignment specimen was employed, 200 mm in length with a 35-mm long reduced gage section and a 6 by 6 mm cross section. Four longitudinal strain gages, equispaced around the circumference, were adhered on two separate longitudinal planes for a total of eight strain gages. Proper load train alignment helps to reduce the introduction of bending moments (and nonuniform stresses) into the specimen during a tension test.

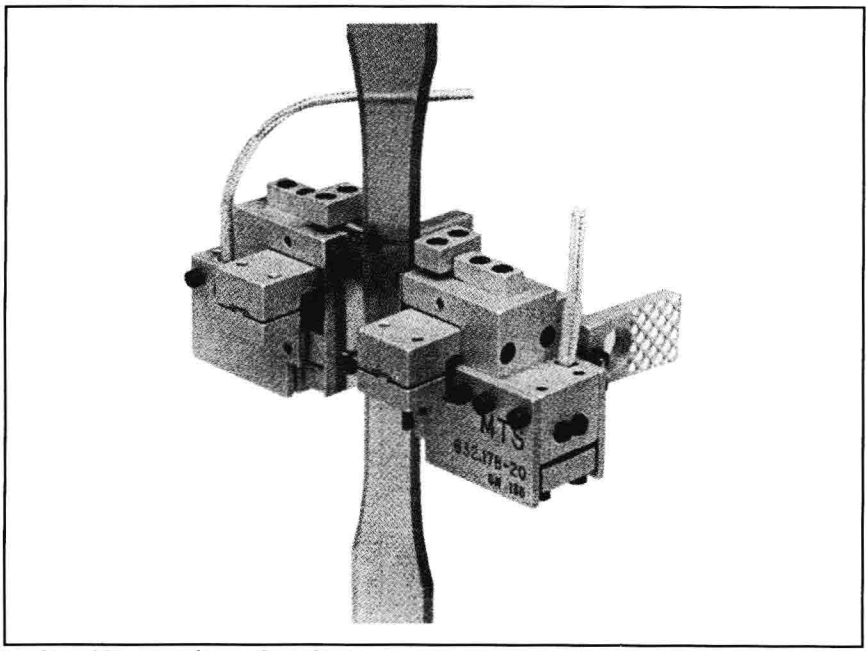

FIG. 2--Illustration of a dual extensometer mounted on a polymer specimen. For tests of CFCCs the extensometer was mounted on the specimen faces.

Separate, continuous strain readings were recorded for two opposing faces of the specimen using a dual-arm, strain-gage based extensometer, Axis A and Axis B, over gage lengths of 25 mm and a range of +50000 x 10^{-6} to -20000 x 10^{-6} m/m strain (Fig. 2). Percent bending (in this case, out of plane bending only) was calculated as:

$$PB = 100\frac{(\varepsilon_A - \varepsilon_B)}{(\varepsilon_A + \varepsilon_B)} \quad (1)$$

where PB is percent bending, ε_A is the strain from Axis A, and ε_B is the strain from Axis B.

A preliminary tension test of one specimen (RG1 geometry) resulted in an ultimate strength of ~250 MPa and a strain at fracture of ~6000 x 10^{-6} m/m. These values were used to approximate times to failure for various test mode and test rate combinations (Table 1). To study the effect of test rate an order of magnitude difference was chosen between the minimum and maximum test rates. Similar rates were chosen to compare differences in test mode. Therefore, establishing times to failure for each geometry was necessary to compare strength and strain results. The final load (500 and 50 N/s) and crosshead displacement rates (0.03 and 0.003 mm/s) were chosen to produce failure times of ~20 and ~200 s.

TABLE 1--Estimated times to failure for various test modes and rates

Geometry	Displacement Control		Load Control	
	0.003 mm/s	0.03 mm/s	50 N/s	500 N/s
RG1, V1=L2*W2	240 s	24 s	180 s	18 s
RG2, V2=L2*W1	340 s	34 s	90 s	9 s
RG3, V2=L1*W2	124 s	12 s	180 s	18 s
SS, V1=L2*W2	180 s	18 s	180 s	18 s

Note: RG (reduced gage), SS (straight sided), volume gage sections, V1 and V2 are computed with: L1 = 30 mm, L2 = 60 mm, W1 = 5 mm, W2 = 10 mm.

RESULTS

Stress-strain Relation

Stress-strain response is the primary means for gathering and analyzing data. The stress-strain response of the test material in this study was generally linear up to the proportional limit stress, σ_O. The proportional limit stress was followed by a nonlinear stress-strain response up to the ultimate tensile strength with stress increasing at a much slower rate than in the linear region. In most cases the stress at fracture corresponded to the ultimate tensile strength. In addition to the proportional limit stress, the elastic modulus, E, ultimate tensile strength, S_U, fracture strength, S_F, and corresponding strain values (ε_O, ε_U, and ε_F), along with the modulus of toughness, U_T, can be represented on a stress-strain curve (Fig. 3). Actual curves of stress versus strain with superposed curves of percent bending versus strain for two specimens of the same geometry are shown in Fig. 4. Two specimens (i.e., one test with replication) were tested at each combination of geometry, test mode, and test rate.

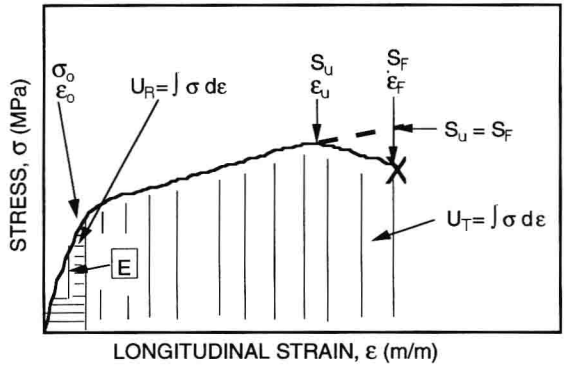

FIG. 3--Generic stress-strain curve and related mechanical properties (ASTM C 1275).

Elastic Modulus

For consistency, elastic modulus for each test was calculated from the slope of the linear, least-squares regression of the stress-strain curve from 0 to 15 MPa. The upper stress value of 15 MPa was used as it represented the least value of the onset of non linearity observed in previous tests. Therefore, it was assumed that all test exhibited a linear region from 0 to 15 MPa. Test results for elastic modulus have been reported previously [6].

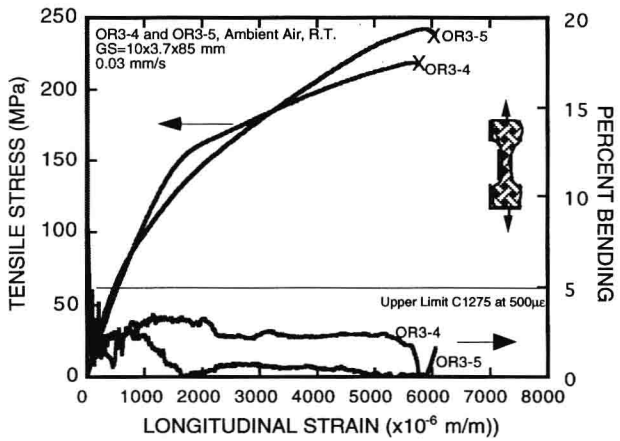

FIG. 4--Actual stress-strain and percent bending-strain curves.

Proportional Limit Stress

ASTM C 1275 recommends two methods for determining the proportional limit (PL) stress (i.e., PL is the stress at an offset strain and PL is stress at a prescribed strain). However, out of five different methods applied to the test data [6], for reasons of consistency, objectivity and numerical efficiency, the proportional limit stress in this study was calculated as follows:

$$\sigma = PL = \sigma_o \text{ when } \frac{(\sigma_i - \sigma)}{\sigma} x100 \geq 10\% \quad (2)$$

where σ_i is the stress calculated from the elastic modulus, E, and the corresponding strain, ε_i, at the i^{th} datum such that $\sigma_i = E\varepsilon_i$, and σ is the actual stress at the i^{th} strain. The proportional limit is the point at which the difference between the actual stress and the calculated stress is equal to or greater than 10%. It can be argued that the proportional limit is the most important design parameter for CFCCs because it defines the stress or strain at the onset of nonlinearity. When specimen geometries are grouped (Fig. 5a) specimen RG1 has the most consistent proportional limit values regardless of test rate or control with specimen RG2 having the overall greatest average value. Comparing test mode and test rate (Fig. 5b) shows that displacement control often results in greater proportional limits than load control.

Ultimate Tensile Strength

In the case of ultimate tensile strength, S_U, both the specimen geometry and test mode/rate relations show fairly consistent results (Fig. 6). The ultimate tensile strength is an important parameter when comparing most materials and can be used intuitively to compare and select a material for "engineering" design. At the ultimate tensile strength, the load is carried almost entirely by the fibers and therefore often coincides with the fracture strength, S_F, of the composite. Although the load is carried by the fibers at S_U, an accurate measure of the in situ fiber strength is difficult since physical and chemical degradation may occur during fabrication [12].

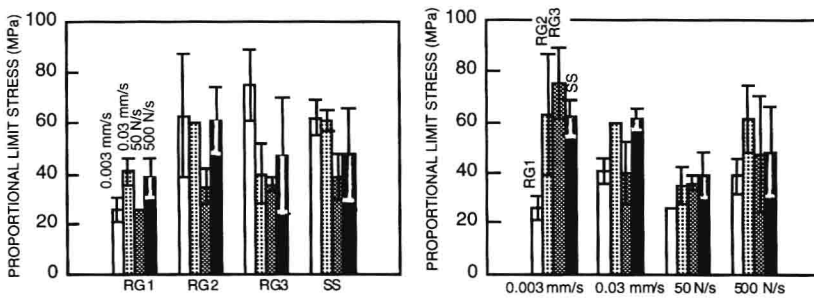

a) Specimen geometry effect on σ_O b) Test mode/rate effect on σ_O

FIG. 5--Effect of test parameters on the proportional limit stress (error bars represent the upper and lower range of the data).

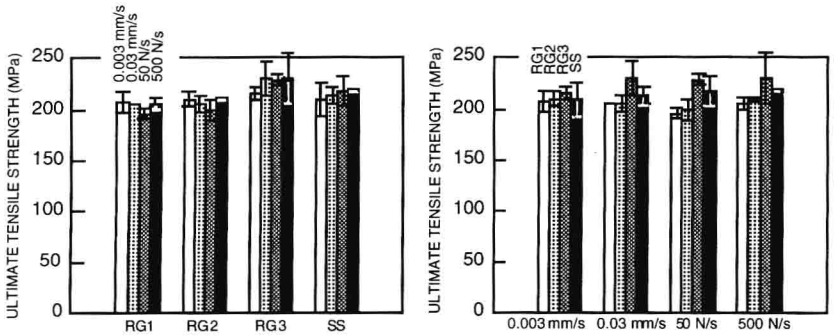

a) Specimen geometry effect on S_U b) Test mode/rate effect on S_U

FIG. 6--Effect of test parameters on the ultimate tensile strength (error bars represent the upper and lower range of the data).

Effect of Percent Bending, PB

The use of a dual-arm extensometer made it possible to calculate the amount of out-of-plane bending in each specimen during each test. PB was calculated to determine the effect of the nonuniformity of uniaxial tensile stress on the calculated material properties. Figure 7 contains all data points represented as a scatter plot to illustrate the effect of percent bending on proportional limit stress and ultimate tensile strength. Data points in Fig. 7 are grouped well around the 1 to 5 PB range. Proportional limit stress (~matrix cracking stress), as expected for the fracture stress of a brittle matrix, decreases with increasing percent bending. Ultimate tensile strengths of 200 to 250 MPa show little effect of increasing percent bending, as expected for the fiber-dominated ultimate tensile strength. Note that trend lines in Fig. 7 are guides for the eye and not curve fits.

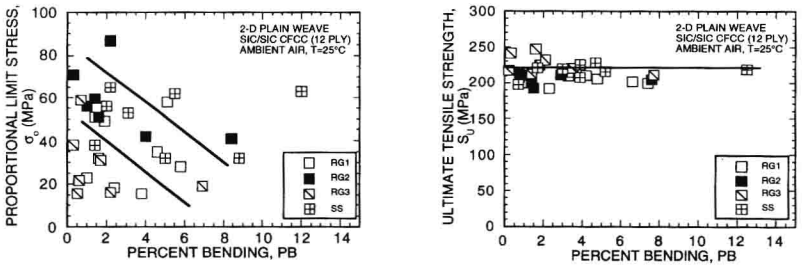

a) Proportional limit stress b) Ultimate tensile strength

FIG 7--Strength as a function of percent bending (a) proportional limit stress and (b) ultimate tensile strength. Note that trend lines are guides for the eye and not curve fits.

Modulus of Toughness and Failure Location

Figure 8 illustrates the scatter for the modulus of toughness (i.e., the total energy absorbed during the tensile deformation and failure of the material), U_T, in relation to the fracture location, l_f, of each specimen. U_T seemed to be more consistent as fracture occurred nearer to the midpoint of the specimen, which is consistent with $U_T = f(\varepsilon)$. U_T as defined mathematically (total area under the tensile stress-strain curve) can be approximated by numerical integration such that:

$$U_T = \int_0^{\varepsilon_f} \sigma \, d\varepsilon \approx \sum_{i=2}^{n} \frac{\sigma_i + \sigma_{i-1}}{2} (\varepsilon_i - \varepsilon_{i-1}) \tag{3}$$

where ε_f is the strain at fracture and σ and ε are the stress and strains from the stress-strain curves, respectively, i is the individual σ and ε data pair, and n is the total number of data pairs.

DISCUSSION

Analysis of Variance

Because of the limited number of replicate tests a statistical analysis of the data was performed to identify the effects of test mode, test rate, and specimen geometry. Specifically, a two-way analysis of variance (ANOVA) with replication [13, 14] capable of evaluating more than one hypothesis simultaneously was performed to determine the effect

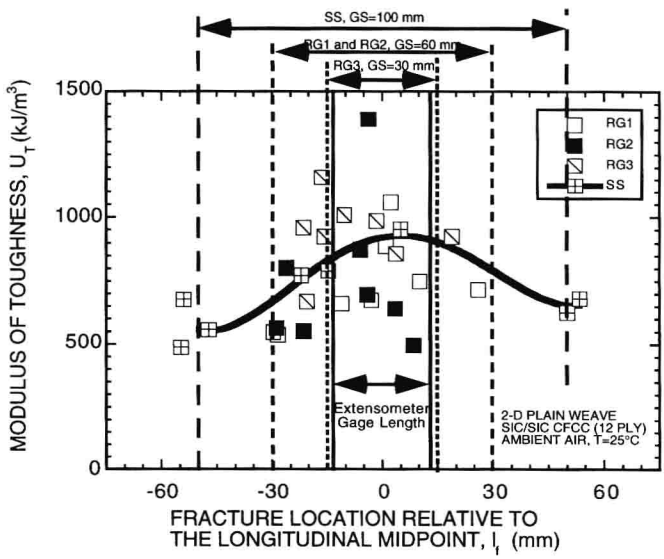

FIG 8--Modulus of toughness for each geometry with respect to fracture location